Laboratory study of wave turbulence under isotropic forcing

Taebel, Z.; McAllister, M. L.; Scotti, A.; Onorato, M.; Van Den Bremer, T. S.

DOI
10.1103/PhysRevFluids.9.094803

Publication date
2024

Document Version
Final published version

Published in
Physical Review Fluids

Laboratory study of wave turbulence under isotropic forcing

Z. Taebel [1,*] M. L. McAllister [2] A. Scotti [3] M. Onorato [4] and T. S. van den Bremer [5]

[1]*Department of Earth, Marine and Environmental Sciences, The University of North Carolina at Chapel Hill, Chapel Hill, North Carolina 27514, USA*

[2]*Department of Engineering Science, University of Oxford, Oxford OX1 3PJ, United Kingdom*

[3]*School for the Engineering of Matter, Transport and Energy, Arizona State University, Tempe, Arizona 85287, USA*

[4]*Dipartimento di Fisica, Università di Torino and INFN, Sezione di Torino, Via Pietro Giuria 1, 10125 Torino, Italy*

[5]*Faculty of Civil Engineering and Geosciences, Delft University of Technology, 2628 CD Delft, The Netherlands*

(Received 10 April 2024; accepted 24 July 2024; published 19 September 2024)

The statistical treatment of random weakly nonlinear interactions between waves, called wave turbulence (WT), is fundamental to understanding the development of the ocean surface. For gravity waves, wave turbulence predicts a dual (direct and inverse) cascade of energy and wave action, which yield power-law solutions for the energy spectrum. While energy cascades were predicted more than 50 years ago, observing them in the laboratory with mechanical forcing remains a challenge. Here, we present experiments in which we attempted to reproduce both direct and inverse cascades in a large circular wave tank. The geometry of the wave tank allows for the creation of isotropically spread surface waves, which is an assumption that underlies WT theory. Although we did see evidence of a direct cascade of energy, we did not observe an inverse cascade of wave action. We discuss the competing effects of dissipation and intermittency, which may dominate or obscure the weakly nonlinear dynamics.

DOI: 10.1103/PhysRevFluids.9.094803

I. INTRODUCTION

The ocean surface involves wave dynamics covering a vast range of spatial and temporal scales. Wind flow over the surface produces waves within a certain scale range (wavelengths on the order of centimeters to hundreds of meters [1,2]). New waves within this scale range, as well as waves outside of it, are produced through nonlinear interactions [1,3]. This process is described by wave turbulence (WT), which is a weakly nonlinear theory involving resonances between linear waves over timescales longer than the wave periods [4]. WT shares several similarities with traditional turbulence, namely, a nonlinear mechanism of cascading conserved quantities across scales, and associated spectral power laws [5].

The cascade is produced through wave-wave interactions. These are processes that transfer energy from existing to new waves [6], provided they satisfy the resonance condition. For surface gravity waves, the resonant manifold compatible with the dispersion relation of deep-water waves comprises wave quartets whose wavenumbers and frequency satisfy

$$\mathbf{k}_1 + \mathbf{k}_2 = \mathbf{k}_3 + \mathbf{k}_4, \quad \omega_1 + \omega_2 = \omega_3 + \omega_4. \tag{1}$$

*Contact author: taebel@live.unc.edu

The theory of WT is developed under the assumptions of weak nonlinearity, a large domain (so that wavenumbers can be thought as continuously distributed), and isotropy [1]. Provided those conditions are met, four-wave interactions evolve the wave action spectrum in accordance with an integrodifferential equation known as the wave kinetic equation (WKE) [7]. For surface gravity waves, there are two power-law energy spectra giving rise to stationary solutions to the WKE: the Zakharov-Filonenko (ZF) spectrum $E_f \sim f^{-4}$ and the Zakharov-Zaslavskii spectrum $E_f \sim f^{-11/3}$ [1], where f is the frequency. The former power law corresponds to a forward cascade of energy and the latter corresponds to an inverse cascade of wave action.

Validating the predictions of WT theory has proven challenging in laboratory experiments and numerical simulations. In a finite-size wave tank, geometric modes form based on the tank shape, and the resulting energy transfer may be suppressed. These finite-size effects tend to produce power laws that are steeper than the WT predictions [8]. There is currently no general theory for discrete WT [1,9], but the physical remedy lies in increasing the nonlinearity of the system; nonlinearity broadens the resonance condition to allow quasiresonant interactions [10], which increases the number of quartets of waves. In fact, previous experimental work has shown that the observed spectra tend towards f^{-4} as the wave steepness increases [4,11–15].

However, increasing the nonlinearity to generate resonances contradicts the theory of WT: the theoretical power laws are independent of the forcing [16], and furthermore one expects to recover the WKE under vanishing nonlinearity [17]. Beyond this discrepancy, the need for nonlinear forcings can lead to misleading results: a wave field of stronger nonlinearities is expected to have a spectral power law f^{-4} known as the Kuznetsov spectrum [18], which is identical to the ZF spectrum (in frequency but not in wavenumber), even though the spectra arise from disparate dynamics [1]. Thus, a tendency toward f^{-4} under stronger nonlinearities may not be due to increasing the availability of four-wave interactions.

The aforementioned issues typically affect the direct cascade, but the inverse cascade suffers from additional obstacles. Such a cascade requires high-frequency forcing and a large domain to accommodate the longer waves produced. Numerical simulations have recently become sufficiently resolved to observe the inverse cascade [19–21], but laboratory evidence remains scarce, with the most successful results found in Falcon *et al.* [22]. The aforementioned work observed the inverse cascade, but questions remain regarding dissipative mechanisms at large scales, and the simultaneous existence of both cascades.

Given the disagreement between experimental work and theory, we set out to determine whether the discrepancies arise because of an inadequate environment for WT to occur. In previous experiments, it was assumed that isotropy arises through wave reflections, since the forcing mechanisms were generally not fully isotropic [4]. In contrast, here we present results from an experimental setup that rigorously enforces the assumptions of WT. This is achieved working in a round tank where the wavemakers are distributed along its perimeter to generate a truly isotropic forcing. We further impose the requirements on nonlinearity and random phases in our input signal. Our setup considers two regimes: a low-frequency forcing meant to observe the direct cascade inertial range and a high-frequency forcing meant to observe the inverse cascade inertial range. We perform a parameter sweep over the remaining forcing parameters, steepness, and spectral bandwidth, to identify the spectral dependence on the wave generation. The experimental setup is presented in Sec. II. We discuss results in Fourier space in Sec. III A. We then turn our attention towards real-world effects that arise in a physical laboratory: we discuss dissipation in Sec. III B and intermittency in Sec. III C. Finally, we draw conclusions in Sec. IV.

II. EXPERIMENTAL SETUP

We performed experiments at the FloWave Ocean Energy Research Facility at the University of Edinburgh (see Fig. 1). The facility features a 25-m-diameter circular wave with a depth of 2 m. 168 independent wavemakers, each capable of forcing waves with frequencies between 0.2 and 2 Hz, are located along the tank perimeter. In normal operation, the wavemakers use a force-feedback

FIG. 1. The FloWave Ocean Energy Research Facility (photograph © David Morris).

control strategy to absorb incident waves; this is used to avoid the buildup of reflected waves in the circular tank. In our experiments, this feature is turned off to prevent external dissipation, and the wavemakers are operated using a position control strategy. The facility has been previously used for studies on highly spread and crossing sea conditions [23,24]; in our case, we employ a forcing from all directions to create an isotropic sea.

The desired wave field is defined as a linear summation of discrete plane-wave components or fronts,

$$\eta(\mathbf{x}, t) = \sum_{n=1}^{N} a_n \cos(\mathbf{k}_n \cdot \mathbf{x} - \omega_n t - \zeta_n), \tag{2}$$

where a_n, $\mathbf{k}_n$, ω_n, and ζ_n are the discrete amplitude, wavevector, frequency, and phase of each front, respectively. The angular frequency ω_n is related to the magnitude of the wavenumber $k_n = |\mathbf{k}_n|$ by the linear dispersion relation $\omega_n = \sqrt{g k_n \tanh(k_n h)}$. WT theory is derived on the assumption that the wave spectrum is isotropic and that the wave field is homogeneous. To create these conditions, we randomly sample directions $\theta_n = \arg(k_n)$ and phases ζ_n from a uniform distribution for each wave front. We use a Gaussian distribution to define the amplitudes of the waves to produce a forcing that is localized in frequency space,

$$a_n = \frac{1}{\Delta f \sqrt{2\pi}} \exp\left(-\frac{1}{2}\frac{(f_p - f)^2}{\Delta f^2}\right)\delta f, \tag{3}$$

where we use the parameters f_p and Δf to set the peak frequency and bandwidth of our forcing. The frequency resolution $\delta f = 1/T$ is determined by the duration of the experiments ($T = 30$ min).

We recorded the surface elevation using eight resistive wave gauges mounted on a gantry over the center of the tank. The gauge positions were chosen pseudorandomly, in that the actual positions were chosen randomly, but subject to the requirement that the distances between the gauges covered the relevant length scales (4 cm to 2 m) of the resulting wave field [25]. We used the gauge positions for directional analysis to verify that our forcing was isotropic, which is not presented here. The gauges sampled at a rate of 128 Hz.

To assess the impact of the forcing parameters on the turbulent cascade, we varied the peak forcing frequency, the forcing bandwidth, and the steepness (see Table I). We performed experiments with two peak frequencies, $f_p = 0.9$ Hz and $f_p = 1.6$ Hz. The experiments with lower-frequency forcing are referred to as direct cascade (DC) experiments, and those with a higher frequency forcing are referred to as inverse cascade (IC) experiments, as the two forcing frequencies will favor the observation of either cascade. The wave steepness ε is defined as $\varepsilon = k_p H_S/2$, where k_p is the peak wavenumber of the forcing and H_S is the significant wave height.

TABLE I. Parameters for each experiment, where f_p is the peak frequency of the Gaussian amplitude spectrum, Δf is the standard deviation of the Gaussian amplitude spectrum in frequency, and $\tilde{f}$ is the normalized bandwidth $\Delta f/f_p$ and defines the narrow (N), medium (M), and broad (B) forcing conditions. H_S is the significant wave height for the input wave field and ε is the input wave steepness defined as $\varepsilon = k_p H_S/2$.

Name	f_p(Hz)	Δf(Hz)	$\tilde{f}$	H_S(m)	ε
N-DC1	0.90	0.02	0.022	0.02	0.03
N-DC2	0.90	0.02	0.022	0.04	0.06
N-DC3	0.90	0.02	0.022	0.05	0.08
N-DC4	0.90	0.02	0.022	0.06	0.10
N-DC5	0.90	0.02	0.022	0.09	0.14
M-DC1	0.90	0.09	0.100	0.02	0.03
M-DC2	0.90	0.09	0.100	0.04	0.06
M-DC3	0.90	0.09	0.100	0.05	0.08
M-DC4	0.90	0.09	0.100	0.06	0.10
M-DC5	0.90	0.09	0.100	0.09	0.14
B-DC1	0.90	0.18	0.201	0.02	0.03
B-DC2	0.90	0.18	0.201	0.04	0.06
B-DC3	0.90	0.18	0.201	0.05	0.08
B-DC4	0.90	0.18	0.201	0.06	0.10
B-DC5	0.90	0.18	0.201	0.09	0.14
B-DC6	0.90	0.18	0.201	0.11	0.18
M-IC1	1.60	0.16	0.100	0.04	0.06
M-IC2	1.60	0.16	0.100	0.06	0.10
M-IC3	1.60	0.16	0.100	0.09	0.14
M-IC4	1.60	0.16	0.100	0.11	0.18
M-IC5	1.60	0.16	0.100	0.13	0.22
M-IC6	1.60	0.16	0.100	0.16	0.26

To ensure consistency between the DC and IC experiments, we defined a normalized forcing frequency bandwidth $\tilde{f} = \Delta f/f_p$. For the DC experiments, we considered three values of $\tilde{f}$: 0.022, 0.100, and 0.201. These defined a narrow, medium, and broad forcing, respectively. The corresponding values of Δf are similar to those of [26], but adapted for f rather than k. For each bandwidth $\tilde{f}$, we performed experiments with five steepness values ε ranging from 0.03 to 0.14, with an additional experiment with $\varepsilon = 0.18$ done for the broad DC experiment. For the IC experiments, we only considered the medium forcing bandwidth $\tilde{f} = 0.100$. However, we performed experiments with six values of ε that ranged from 0.06 to 0.26. Individual forcing parameters are shown in Table I.

Each individual experiment lasted 30 min, which we believe is a sufficient time to observe a turbulent cascade, based on preliminary experiments. The gauges recorded continuously during this interval and continued sampling for an additional 30 min after the forcing stopped. This spin-down time allowed the tank to revert back to a quiescent state before the start of the next experiment. We mention that the energy accumulation in the DC wave field produced values of H_S considerably larger than the values we expected based on the forcing intensity. The wave heights grew until they finally reached a nearly statistical stationary state toward the end of the experiment, as shown for all three DC forcing bandwidths in Fig. 2. In contrast, during the IC experiments, the recorded significant wave heights were the same as that expected from the forcing intensity. We are not certain of the mechanism that leads to a greater accumulation of energy in the DC experiments. We hypothesize this could be due to either the greater difference between input frequency and the high-frequency part of the spectrum where dissipation (hypothetically) takes place for the DC experiments or the higher energy flux into the tank (for the same amplitude forcing) for the DC

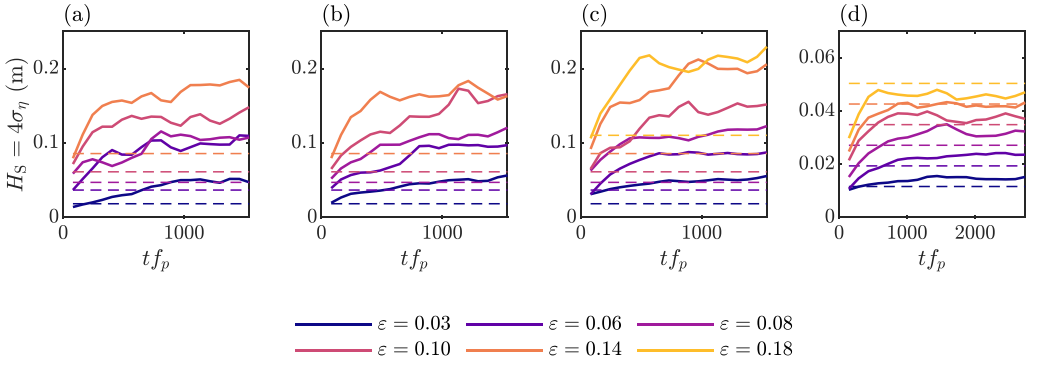

FIG. 2. Significant wave height H_S for (a) N-DC (narrow-bandwidth forcing), (b) M-DC (medium-bandwidth forcing), (c) B-DC (broad-bandwidth forcing), and (d) M-IC (medium-bandwidth forcing) for each value of ε. The significant wave height H_S is calculated as $4\sigma_\eta$ for all gauges over 3-min windows with 50% overlap. The dashed lines correspond to input values of H_S listed in Table I. Time is normalized by the peak frequency of each forcing f_p.

experiments, which are associated with a larger group velocity (energy flux is proportional to group velocity or a combination of the two effects.

An example surface elevation time series is shown in Fig. 3(a), taken from M-DC4 over the final 5 min of wavemakers activity. We see evidence of nonlinearity in the wave field through the distribution of normalized surface elevation η/σ_η, where σ_η is the standard deviation of surface elevation. The distribution of η from Fig. 3(a) is shown in Fig. 3(b), which we compare to a Gaussian distribution and a Tayfun distribution. The latter is defined in asymptotic form by Socquet-Juglard *et al.* [27] as

$$P(\eta) = \frac{1 - \frac{7\sigma_\eta^2 k_p^2}{8}}{\sqrt{2\pi(1 + 3G + 2G^2)}} \exp\left(\frac{-G^2}{2\sigma_\eta^2 k_p^2}\right), \quad G = \sqrt{1 + 2k_p\sigma_\eta\eta} - 1, \tag{4}$$

where k_p is the spectral peak wavenumber. Our experiments deviate from the Gaussian distribution for surface elevation and agree well with the Tayfun distribution, which indicates that second-order effects are finite in our wave field.

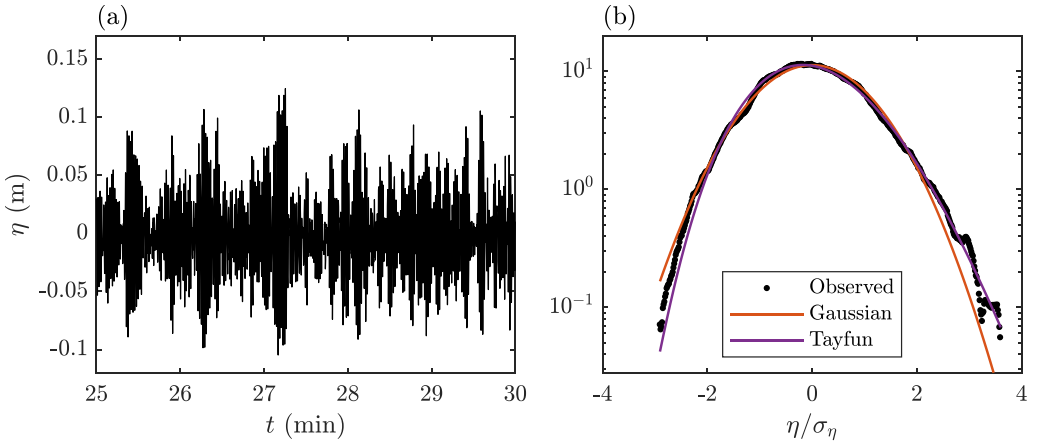

FIG. 3. (a) Surface elevation η taken from M-DC4 from a single gauge over the final 5 min during wavemaker forcing. (b) Normalized histogram of surface elevation η for the period shown in (a) compared to a Gaussian distribution, and Tayfun distribution calculated with Eq. (4) using measured values of σ_η and k_p.

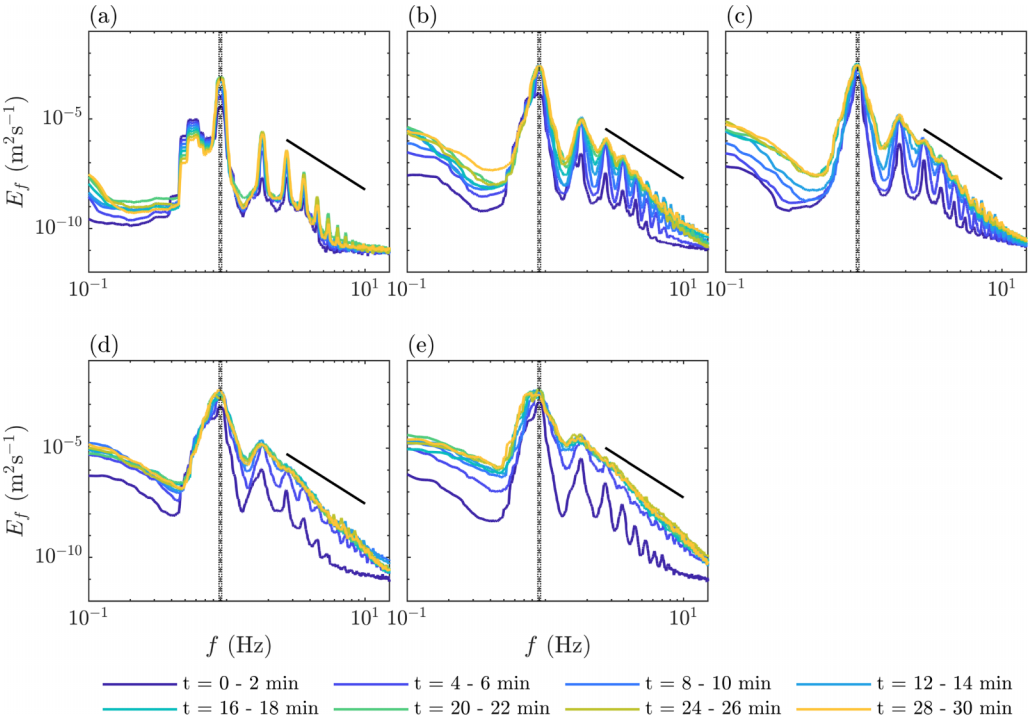

FIG. 4. Surface elevation energy spectra calculated over 2-min windows for N-DC (narrow-bandwidth forcing) with (a) $\varepsilon = 0.03$, (b) $\varepsilon = 0.06$, (c) $\varepsilon = 0.08$, (d) $\varepsilon = 0.10$, and (e) $\varepsilon = 0.14$ during wavemaker forcing. Spectra are averaged over all wave gauges and smoothed using a moving mean of length 0.1 Hz. The black central dashed line is f_p; the left and right vertical dashed lines are $f_p \pm \Delta f$. The solid black line corresponds to the Zakharov-Filonenko prediction f^{-4}.

III. RESULTS

A. Spectral analysis

We start by presenting the spectral results for the suite of experiments conducted, focusing first on the DC experiments during the duration of the forcing. To illustrate how spectral evolution changes with forcing intensity and bandwidth, we present spectra taken over 2-min windows during the 30 min of forcing for each of the experiments. Based on the results we present, we define the inertial range of the DC experiments to be between 3 and 8 Hz, while for the IC experiments we define it as between 4 and 8 Hz. All spectra are smoothed with a moving mean of length equal to 2% of the length of the corresponding inertial range.

Starting with the N-DC experiments, shown in Fig. 4, we can see a clear dependence of the spectra on the nonlinearity of the forcing. For the lowest steepness forcing, the initial harmonic structure of the spectrum does not change with time, power-law tails do not form, and there is very little energy at high frequencies. As the forcing steepness increases, the harmonic peaks gradually broaden leading to a more continuous spectrum, with the highest intensity experiments forming a smooth power-law tail by the end of the 30 min. The resulting power-law slopes are steeper than the predicted -4 value, and begin well beyond the forcing frequency ($\approx 3 f_p$). Figure 5 shows the spectral evolution for the M-DC experiments. Similarly to the N-DC wave field, the lower steepness forcing spectra have a harmonic structure, albeit less pronounced than those for the N-DC. While the lowest intensity N-DC spectrum featured harmonics over nearly a decade in frequency, the energy contained in the harmonics decreases more quickly for the M-DC spectrum. Additionally, a smooth

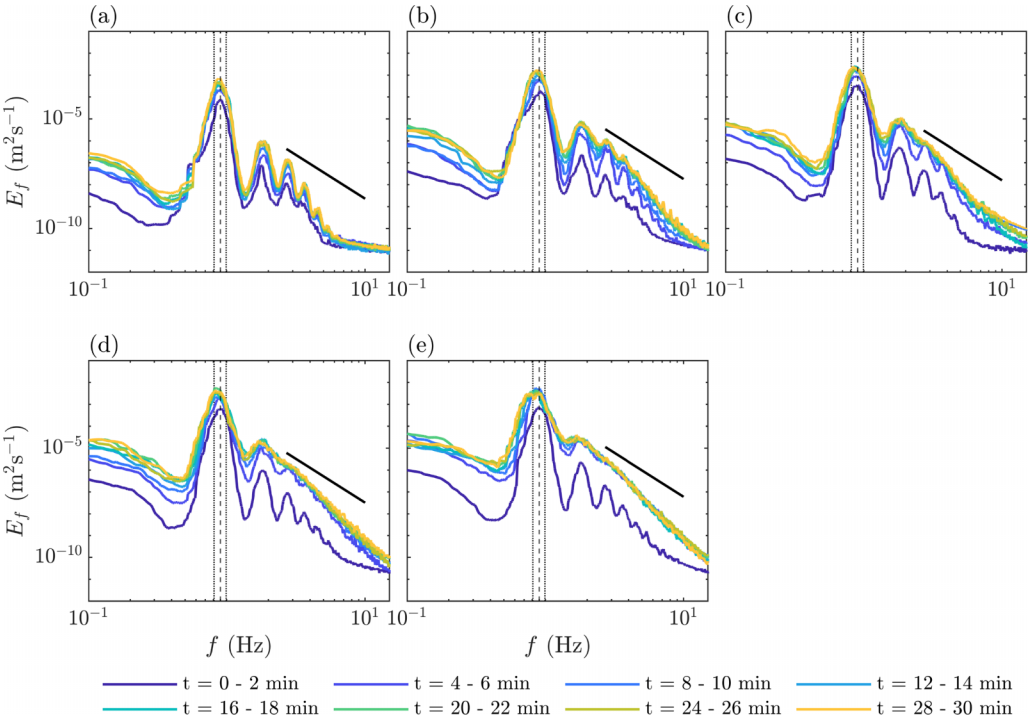

FIG. 5. Surface elevation energy spectra calculated over 2-min windows for M-DC (medium-bandwidth forcing) with (a) $\varepsilon = 0.03$, (b) $\varepsilon = 0.06$, (c) $\varepsilon = 0.08$, (d) $\varepsilon = 0.10$, and (e) $\varepsilon = 0.14$ during wavemaker forcing. Spectra are averaged over all wave gauges and smoothed using a moving mean of length 0.1 Hz. The black central dashed line is f_p; the left and right vertical dashed lines are $f_p \pm \Delta f$. The solid black line corresponds to the Zakharov-Filonenko prediction f^{-4}.

tail forms earlier than for the narrow forcing, as seen in the higher steepness experiments, where the harmonics are no longer visible by the 5-min mark for the highest-intensity forcing. The spectral shape evolves into a power law earlier, but again the observed slopes are steeper than -4.

Shifting to the B-DC experiments, the reduction in harmonic structure from narrow to medium forcing continues here, as even at the lowest-intensity forcing the harmonic peaks are broader. As forcing intensity increases, the harmonic peaks smooth out more quickly than previously, and a power law begins to form for the more nonlinear experiments. Again, the slopes are steeper than expected. We also note that the B-DC experiments showed a slight downshifting of the peak frequency. As seen in Fig. 6, the spectral peak shifts to lie near the lower bound of the forcing range, unlike in the narrower-bandwidth experiments discussed above.

These results show that a broader forcing tends to yield a smoother spectrum at higher frequencies. As in prior work, we also observe that stronger forcing intensities yield more well-developed power laws. To investigate the relation between the forcing intensity and the resultant power law, in Fig. 7 we plot the slope of the high-frequency spectral tails; we measure ν as a function of ε, measured over the final 5 min of the experiment, when the wave field has reached a steady state. Since not all experiments developed a coherent power law, we only consider the slopes for the higher steepness experiments. As seen in Fig. 7, the high-frequency spectral tails generally become steeper as ε increases. This result agrees with previous experimental work [11]. However, in our case, ν is minimized at a value of -6. This is steeper than f^{-4} ($\nu = -4$), but agrees better with mesoscopic turbulence theory [1], which is expected for a wave system when finite-size effects are significant.

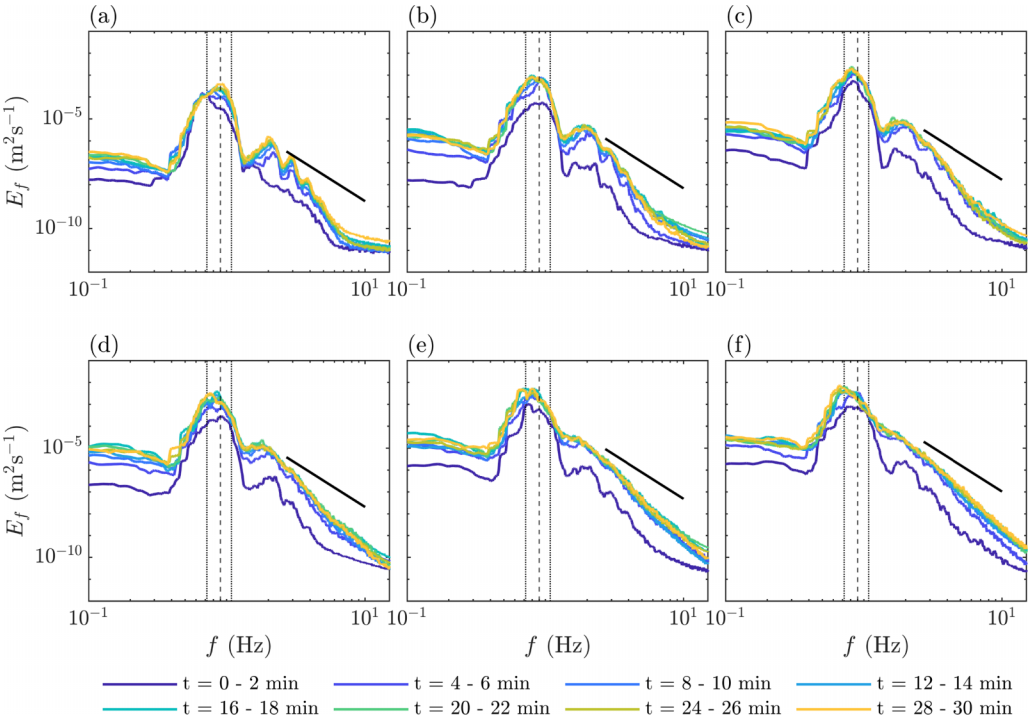

FIG. 6. Surface elevation energy spectra calculated over 2-min windows for B-DC (broad-bandwidth forcing) with (a) $\varepsilon = 0.03$, (b) $\varepsilon = 0.06$, (c) $\varepsilon = 0.08$, (d) $\varepsilon = 0.10$, (e) $\varepsilon = 0.14$, and (f) $\varepsilon = 0.18$ during wavemaker forcing. Spectra are averaged over all wave gauges and smoothed using a moving mean of length 0.1 Hz. The central black dashed line is f_p; the left and right vertical dashed lines are $f_p \pm \Delta f$. The solid black line corresponds to the Zakharov-Filonenko prediction f^{-4}.

This is reflected in the accumulation of energy near the forcing frequency, and the lack of energy towards higher frequencies.

Although the spectral slopes we observe are steeper than -4 and are potentially affected by finite-size effects, the formation of a power-law tail at frequencies above forcing is still indicative of nonlinear energy transfer. We can compare this energy transfer with that predicted by WT using the wave energy flux P for our system. WT predicts $P \sim \varepsilon^6$ provided P is smaller than a cutoff $P_c = (g/\omega_p)^3$ at which point WT no longer applies [4,28].

We can determine P following the methods of [22]. Once the wavemakers are shut off, the wave field enters a freely decaying regime. The temporal derivative of the mean gravity wave energy, $E(t) = g\sigma_\eta^2(t)$, is related to P via $P = -dE/dt$ evaluated at $t = t_0$, where t_0 is the shutoff time. We estimate this via the slope of $E(t)$ from our experimental results.

Recalling the character of Fig. 2, the significant wave height is nonconstant and grows over roughly the first 25 min of forcing and exceeds the prescribed value of H_S. Thus, the input value of ε is not representative of our system at the end of the forcing. Since H_S is most stationary during the last 5 min of forcing, we introduce an effective steepness as $\varepsilon_c = \omega_c^2 H_S/(2g)$. Here ω_c is the peak frequency over the last 5 min, calculated following [29] as

$$\omega_p = \frac{m_0^2}{m_1 m_{-2}}, \tag{5}$$

where m_n is the nth spectral moment. All three DC wave fields have fluxes P that increase roughly linearly with ε_c^6, as shown in Fig. 8. We then validate that our values of P satisfy $P < P_c$, and

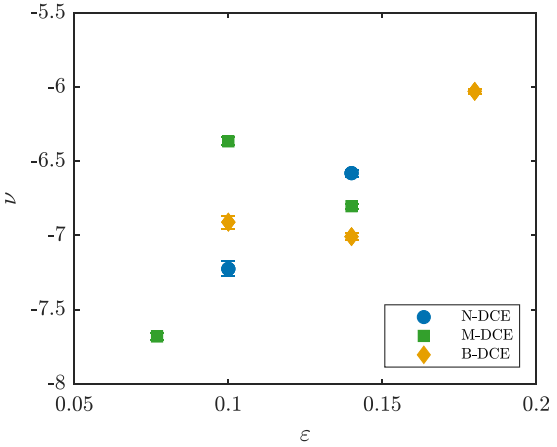

FIG. 7. Exponent of the spectral tail f^{ν} vs input steepness ε for all DC experiments over the final 5 min of wavemaker forcing. Before fitting the exponent, the spectra are averaged over all wave gauges and smoothed with a moving mean of width 0.06 Hz. Error bars are 95% confidence intervals of the power-law fit.

calculate P_c for the DC experiments. We calculate $P_c = 5.2\ \mathrm{m}^3\ \mathrm{s}^{-3}$ so there is roughly five orders of magnitude between our fluxes and the breaking point of WT. This suggests that there is an energy cascade driven by wave-wave interactions. We note, however, that while our relationship between P and ε agrees with WT theory, our relationship between E_f and P does not. The full ZF solution $E_f \sim P^{1/3} g f^{-4}$ [4] shows $E_f \sim P^{1/3}$, which we do not observe in our experiments. Rather we find E_f grows with P faster than $P^{1/3}$. This disagreement is reflected in the difference between our power laws and the theoretical f^{-4}.

We now turn our attention to the spectra from the IC experiments. Compared to the DC spectra, the IC spectra were considerably further removed from WT theory. As before, we first present the temporal evolution of the spectrum over 2-min blocks, shown in Fig. 9. Similar to the DC spectra, the development of a smoother tail at high frequencies accompanies a growth in the steepness of the forcing. At lowest steepness, we again observe a harmonic structure. We briefly pause here to mention that for a WT system with narrow forcing, the resulting comblike spectral peaks are expected to obey power laws in amplitude and width (see Fig 3.14 in Chap. 3 of [30]). Across all

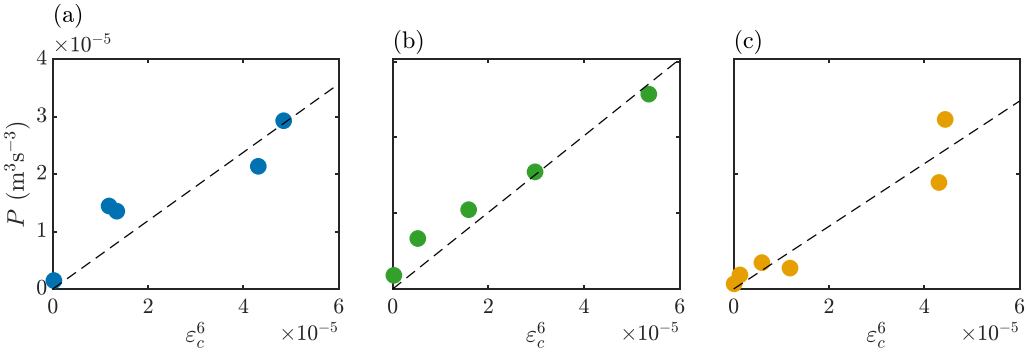

FIG. 8. Energy flux P vs sixth power of calculated wave steepness ε_c^6 for (a) N-DC, (b) M-DC, and (c) B-DC. P is estimated via the decay of gravity wave energy after forcing is stopped and averaged over the gauges. ε_c is calculated over the final 5 min of wavemaker forcing as $\varepsilon_c = k_c H_{S_c}/2$, where H_{S_c} is the calculated significant wave height and k_c is the calculated peak wavenumber corresponding to the calculated peak frequency ω_c from Eq. (5).

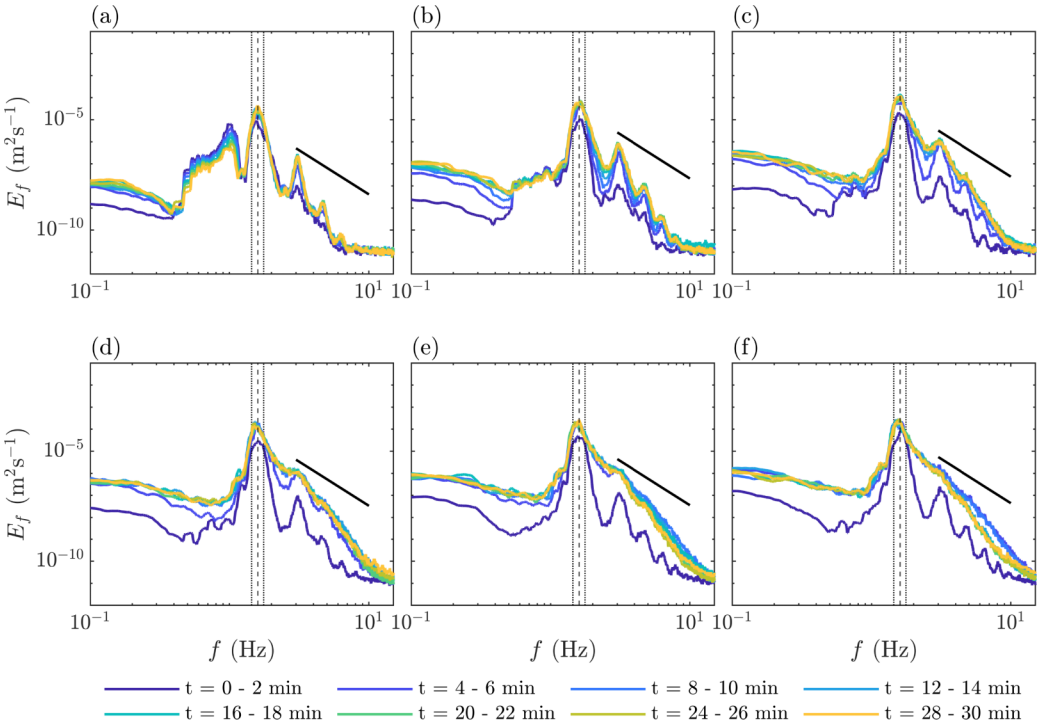

FIG. 9. Surface elevation energy spectra calculated over 2-min windows for M-IC with (a) $\varepsilon = 0.06$, (b) $\varepsilon = 0.10$, (c) $\varepsilon = 0.14$, (d) $\varepsilon = 0.18$, (e) $\varepsilon = 0.22$, and (f) $\varepsilon = 0.26$ during wavemaker forcing. Spectra are averaged over all wave gauges and smoothed using a moving mean of length 0.075 Hz. The central black dashed line is f_p; the left and right vertical dashed lines are $f_p \pm \Delta f$. The solid black line corresponds to the Zakharov-Filonenko prediction f^{-4}.

of our experiments, DC and IC, the harmonic peaks decay in amplitude faster than a power law, while their widths are highly sensitive to the choice of windowing and averaging, and do not follow a consistent scaling. Returning to the M-IC experiments, the low steepness harmonics disappear as the forcing becomes stronger. However, contrary to the DC experiments, the resulting spectral slopes have greater fluctuation across the frequencies of interest and do not present obvious evidence of a power law.

As the intention of the IC experiments was to maximize an inertial range of subharmonics, we turn our attention to the spectral behavior at lower frequencies. We did not observe a clear growth or downshifting of the peak frequency. However, a smooth spectral feature emerged for steeper forcings. In particular, the least steep forcing shows an isolated hump to the left of the forcing range, which is not present in any of the other experiments. Steeper forcings engender a greater drop in spectral energy to the left of the forcing peak, which then becomes a nearly flat spectrum. This suggests that there is an evolution of subharmonics, but not one which exhibits the expected $-11/3$ power law of WT. We note that the spectral slopes observed for low frequencies may be in part due to subharmonic bound waves at second order in steepness, but could also be a manifestation of the inverse cascade in shallow water, which predicts $E_f \sim f^{-1}$ [31], as some of the lower frequencies of the spectrum correspond to shallow-water waves.

B. Spectral decay

After the forcing is stopped, the wave field enters a freely decaying regime, which we record for 30 min before the start of the next experiment. Based on numerical [26,32] and experimental [4,33]

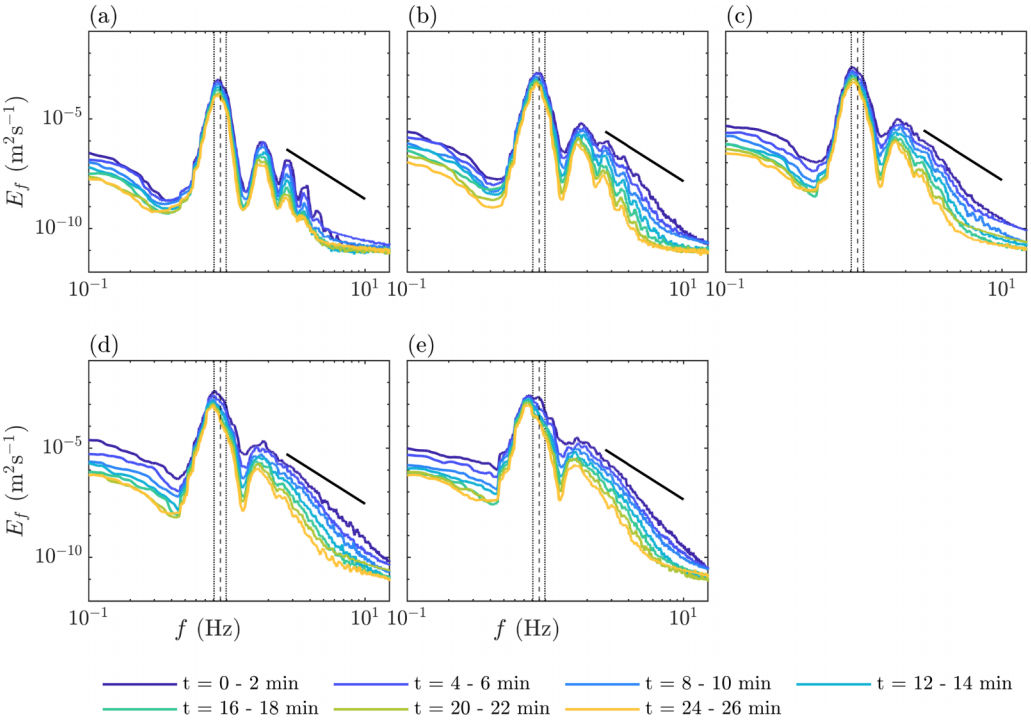

FIG. 10. Surface elevation energy spectra calculated over 2-min windows for M-DC (medium-bandwidth forcing) with (a) $\varepsilon = 0.03$, (b) $\varepsilon = 0.06$, (c) $\varepsilon = 0.08$, (d) $\varepsilon = 0.10$, and (e) $\varepsilon = 0.14$ after wavemaker forcing was stopped. Spectra are averaged over all wave gauges and smoothed using a moving mean of length 0.1 Hz. The central black dashed line is f_p; the left and right vertical dashed lines are $f_p \pm \Delta f$. The solid black line corresponds to the Zakharov-Filonenko prediction f^{-4}.

studies on freely decaying wave turbulence, one would expect a self-similar decay of a power-law spectrum. To illustrate the spectral decay behavior, we show spectra calculated over 2-min windows after the wavemakers were turned off for the M-DC in Fig. 10.The decay of the spectrum clearly is not self-similar, as the spectral slopes steepen dramatically within the inertial range, while the high-frequency tails of the spectra flatten. Of particular note is the reemergence of the initial harmonic structure we saw shortly after the wavemakers were turned on. Compared to Fig. 5 at early t, we see peaks similar to those of Fig. 10 at later t. In the case of the weaker forcings, this is to be expected, given that the harmonic structure never truly bled out. In all cases, the second harmonic becomes more pronounced, driven by a dramatic reduction in energy at frequencies between f_p and $2f_p$. This phenomenon is also clearly observed in the IC spectral decay (Fig. 11). To further analyze the decay, we look at the temporal evolution of individual Fourier amplitudes. We do this via a spectrogram with 8-s windows and 50% overlap. The spectrogram is averaged over the eight gauges for each experiment. A characteristic plot showing the evolution, taken from the M-DC with $\varepsilon = 0.1$, is shown in Fig. 12 for six frequencies. The lowest frequency 0.9 Hz corresponds to the peak of the forcing and then its second harmonic at 1.8 Hz. The frequencies 3, 5, and 8 Hz represent the inertial range. The decay rate generally increases as the frequency is increased from 0.9 to 3 Hz, but then decreases for the higher frequencies within the inertial range. Notable is the decay of the mode at 1.3 Hz, which decays faster than all but the mode at 3 Hz. This frequency corresponds to the behavior between f_p and $2f_p$, which leadsto a reemergence of the second harmonic in Fig. 10. We can quantify the decay rates by fitting a function for $E_f(t)$. Based on WT theory, for small t the loss of energy at a given frequency should be primarily due to four-wave interactions, which gives a

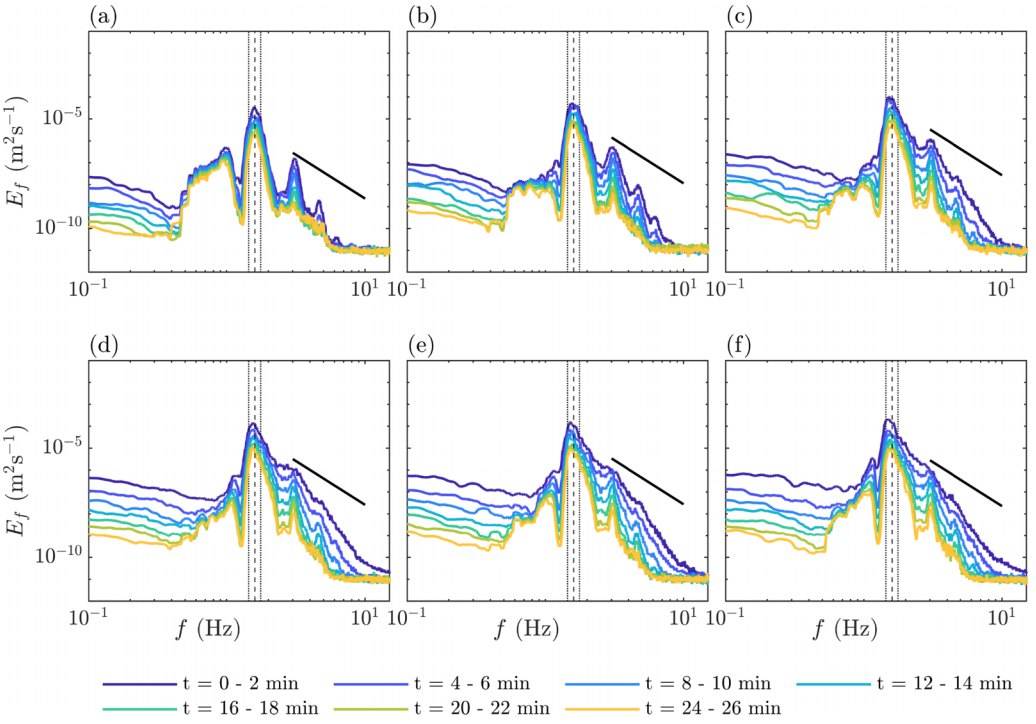

FIG. 11. Surface elevation energy spectra calculated over 2-min windows for M-IC with (a) $\varepsilon = 0.06$, (b) $\varepsilon = 0.10$, (c) $\varepsilon = 0.14$, (d) $\varepsilon = 0.18$, (e) $\varepsilon = 0.22$, and (f) $\varepsilon = 0.26$ after wavemaker forcing was stopped. Spectra are averaged over all wave gauges and smoothed using a moving mean of length 0.075 Hz. The black central dashed line is f_p; the left and right vertical dashed lines are $f_p \pm \Delta f$. The solid black line corresponds to the Zakharov-Filonenko prediction f^{-4}.

power-law scaling $E_f(t) \sim t^{-1/2}$. For large t, dissipation out-competes wave-wave interactions, and the decay should be exponential as $E_f(t) \sim e^{-t/\tau_D(f)}$, where $\tau_D(f)$ is the dissipative timescale for a wave at frequency f [12]. We expect to see a change from the power law to exponential scaling at a crossover time, but in our case, we find that an exponential profile fits well across all t. This contradicts the assumed timescale argument of WT, and suggests that dissipation is more significant than nonlinear interactions in removing energy from the waves.

We calculated $\tau_D(f)$ for all frequencies in each experiment and consistently found the minimum to be near the start of the inertial range, with another local minimum near 1.3 Hz. To illustrate this, we show the calculated values of τ_D taken from the same experiment (M-DC4) as in Fig. 12. This was done with 20-s blocks to improve the frequency resolution of the spectra. To ensure that our calculated values of τ_D are not significantly biased by the initial spectral amplitudes, the spectrogram is normalized by the spectral values for each frequency at $t = t_0$, when the wavemakers are turned off. The results are shown in Fig. 13.

Having dissipation occurring most quickly for waves at low frequencies is surprising, but also concerning. WT assumes that the timescale of nonlinear interactions is much longer than the linear wave periods, but much shorter than the dissipative timescales. We compare the two timescales using the nonlinear timescale for gravity waves

$$T_{\mathrm{NL}} = \frac{2\pi g}{C\omega k P^{2/3}}, \tag{6}$$

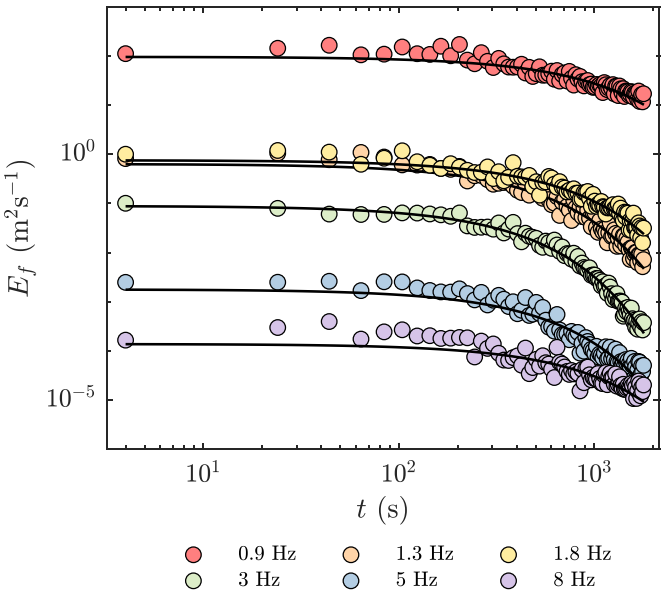

FIG. 12. Temporal decay of five Fourier modes from M-DC4 after wavemaker forcing was stopped. Fourier amplitudes are determined via a spectrogram with 8-s windows and 50% overlap. Black curves correspond to power-law fits for exponential decay e^{-t/τ_D}.

where P is the energy flux [11]. The coefficient C is the Kolmogorov-Zakharov constant [4], which has been estimated to fall between 0.5 [7] and 2.75 [34]. Here, we consider both values as limiting cases and calculate T_{NL} for frequencies within the inertial range. We compare our values of τ_D with those estimated from T_{NL} in Fig. 13. We briefly mention that for either C, T_{NL} is roughly two orders of magnitude larger than the linear wave periods for the range of frequencies considered. The dissipative timescale we calculate is less than the nonlinear timescale for frequencies up to roughly 34.5 Hz, depending on C. This region corresponds to the start of the inertial range and the first stage of the energy cascade. Energy lost to dissipation before it can be transferred to waves with shorter wavelengths may explain why our spectral slopes are steeper than WT theory at high frequencies.

It is also worth noting that, based on Fig. 13, τ_D does not decrease monotonically in f. The quickest decay occurs for frequencies near the beginning of the inertial range, but the decay is nearly as fast at 1.3 Hz. Based on the typical decay rates for a fluid surface, one would expect τ_D to decrease with f, rather than having a minimum at low frequencies [33]. This suggests that our dissipation may not be a simple linear viscous dissipation but may be an artifact of the tank itself. A wave of frequency 1.3 Hz has a wavelength of roughly 1 m, which is similar to the width of two wavemaker paddles. The paddles may function as a resonant damping for waves at this frequency. In all experiments, even those where the forcing frequency was greater than 1.3 Hz (Fig. 11), we found that energy was preferentially dissipated at this frequency.

C. Intermittency

The energy fluxes for our wave field (Fig. 8) suggest that there may be an energy exchange between the waves in accordance with WT theory, but the decay of spectral amplitudes indicates other dynamics at play. These dynamics may be related to finite-size effects, dissipation, or stronger nonlinear behavior. A proper diagnosis would require full spatiotemporal data, but by using higher-order statistics we can investigate the occurrence of stronger nonlinear behavior through intermittency in our wave field. Intermittency is well known in hydrodynamic turbulence as ephemeral bursts of intense motion, which produce significant non-Gaussian statistics [17].

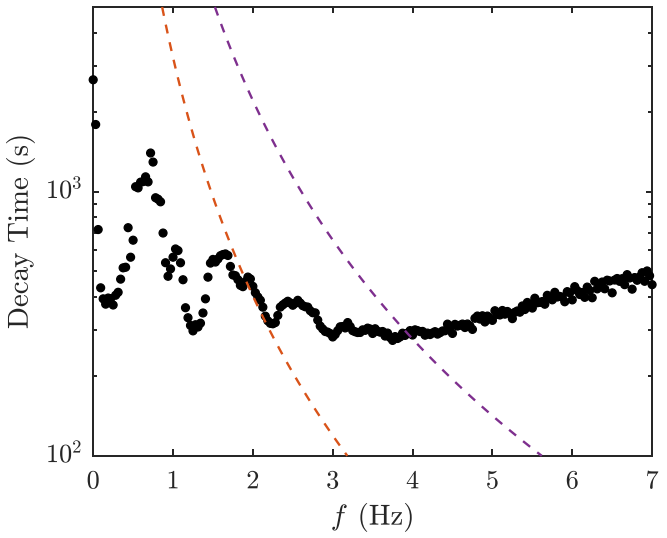

FIG. 13. Dissipative timescale τ_D of Fourier modes from M-DC4 compared to theoretical nonlinear interaction time T_{NL} vs f. Fourier amplitudes are determined via a spectrogram with 20-s windows and 50% overlap. τ_D is determined from an exponential fit e^{-t/τ_D}. The black curves correspond to power-law fits for exponential decay e^{-t/τ_D}. T_{NL} is estimated from 6 using P from Fig. 8(b). The purple dashed curve is T_{NL} with $C = 0.5$; the orange curve is with $C = 2.75$.

Intermittency has also been observed in WT systems [12,13,35–37] as large fluctuations in the wave field.

To test for intermittency, we examine the increments of the surface elevation $\eta(t)$. We denote an increment of order j as $\delta^j_\eta(\tau)$, where τ represents a temporal offset. The first-order increments are defined as $\delta^1_\eta(\tau) = \eta(t+\tau) - \eta(t)$, which are commonly used in hydrodynamic turbulence. In WT, however, the steeper power laws require using higher-order increments. For a system with random phases and an energy spectrum that follows a power law of the form $E_f \sim f^\nu$, the order of increments must be chosen such that $|\nu| > 2j - 1$ in order to address the low-frequency divergence of the spectrum. For surface gravity waves described by the ZF spectrum $E_f \sim f^{-4}$, this means one must use at least second-order increments $\delta^2_\eta(\tau) = \eta(t+\tau) - 2\eta(\tau) + \eta(t-\tau)$ [1].

Our spectra have steeper high-frequency tails than the ZF solution, and thus we choose to work with fourth-order increments, which appeases all of our experiments with an admissible power law. It should be noted that several experiments could have been studied with third-order increments; however, for those experiments we expect the statistics of $\delta^3_\eta(\tau) \approx \delta^4_\eta(\tau)$ [36] and we desire an algorithm that can be applied to all experiments alike. The fourth-order increment is defined as $\delta^4_\eta(\tau) = \eta(t+2\tau) - 4\eta(t+\tau) + 6\eta(\tau) - 4\eta(t-\tau) + \eta(t-2\tau)$.

The first way to check for intermittency is to check the probability density functions (PDFs) of the increments normalized by standard deviation. The expectation is that intermittent signals will deviate strongly from a Gaussian profile at small timescales [38]. For the DC experiments we define the inertial range to be from 3 to 8 Hz, and so the range of τ we consider for $\delta^4_\eta(\tau)$ is defined as $3\ \mathrm{Hz} \leqslant 1/(2\tau) \leqslant 8\ \mathrm{Hz}$; for the IC experiments the reduced inertial range sets $3\ \mathrm{Hz} \leqslant 1/(2\tau) \leqslant 8\ \mathrm{Hz}$ [12]. A characteristic PDF for the DC experiments is shown in Fig. 14(a), taken from M-DC4. The largest deviation of the tails from a Gaussian occurs at small τ, which is characteristic of intermittency [17]. This means that our surface elevations undergo dramatic fluctuations within short timescales. Furthermore, the non-Gaussian profile across all τ indicates that this intermittency is meaningful across the relevant temporal scales corresponding to our inertial range. We mention that these results are consistent with those from N-DC, B-DC, and M-IC experiments.

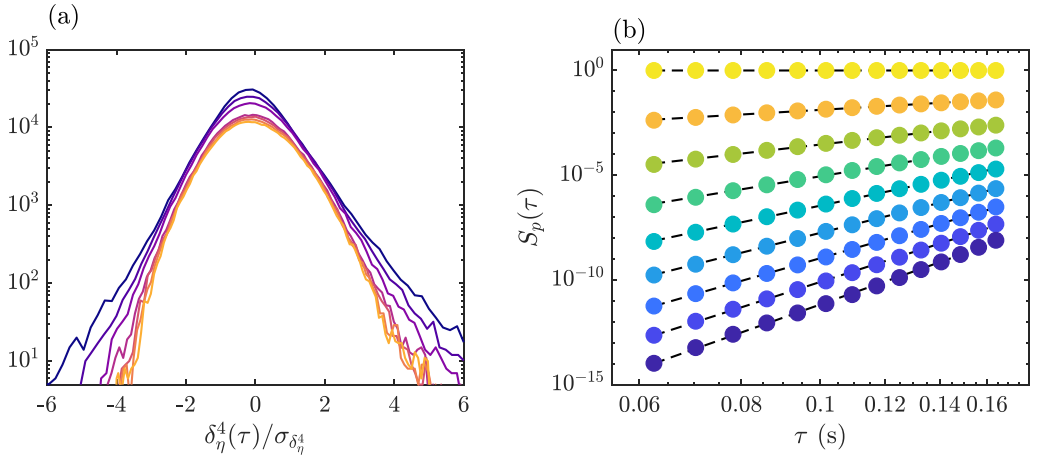

FIG. 14. (a) Normalized histogram of fourth-order increments $\delta_\eta^4(\tau)$ from M-DC4 over the final 5 min of wavemaker forcing. τ ranges from 0.06 s (dark purple) to 0.11 s (light orange) in 0.01-s steps. Increments are individually evaluated for each gauge. (b) Structure functions $S_p(\tau)$ for $p = 0$ (yellow) through 8 (dark blue) vs time lag τ. The values of $S_p(\tau)$ are averaged across all wave gauges. The black dashed lines represent power-law fits $S_p(\tau) \sim \tau^{\zeta(p)}$. Values of τ for both figures are set by the frequencies of the corresponding spectral inertial range.

Beyond just PDFs we can discern the character of intermittency from the moments of the increments, referred to as structure functions. For a given set of surface elevation increments, the structure function of order p is defined as $S_p(\tau) = \langle|\delta_\eta^j(\tau)|^p\rangle$, where $\langle\cdot\rangle$ denotes an average over t. For a stationary random process, a system with a power-law spectrum will in turn have structure functions that follow a power-law scaling in τ as $S_p(\tau) \sim \tau^{\zeta(p)}$. The behavior of $\zeta(p)$ quantifies the intermittent nature of our signal. If we have strictly linear waves with random phases, then from the spectral power law $E_f \sim f^\nu$ of our system we find $\zeta(p) = p(|\nu| - 1)/2$, provided j is large enough for $|\nu| > 2j - 1$. Deviations from this relationship between $S_p(\tau)$ and τ, particularly at high values of p, are evidence of intermittency.

For p from 0 to 8, we calculate $S_p(\tau)$ for each experiment over the final 5 min of active forcing and average the result over all the wave gauges. The relationship between $S_p(\tau)$ and τ is shown for M-DC4 in Fig. 14(b). Within the range of τ associated with the spectral power-law range, we see that $S_p(\tau)$ follows a power-law scaling in τ with a fixed exponent for all p. We fit a power law

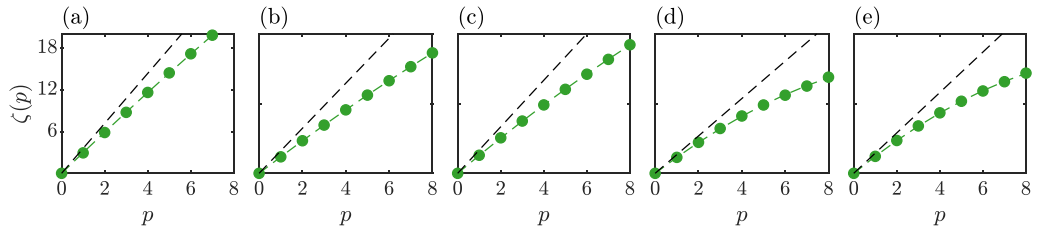

FIG. 15. Structure function power-law exponents $\zeta(p)$ vs p for M-DC with (a) $\varepsilon = 0.03$, (b) $\varepsilon = 0.06$, (c) $\varepsilon = 0.08$, (d) $\varepsilon = 0.10$, and (e) $\varepsilon = 0.14$. Structure functions are calculated over the final 5 min with the forcing on and averaged over all wave gauges. p ranges from 0 to 8. The black dashed line represents theoretical linear scaling $\zeta(p) = p(|\nu| - 1)/2$, with ν taken from Fig. 7. The green dashed curve represents a quadratic fit $\zeta(p) = c_1 p - c_2/2p^2$.

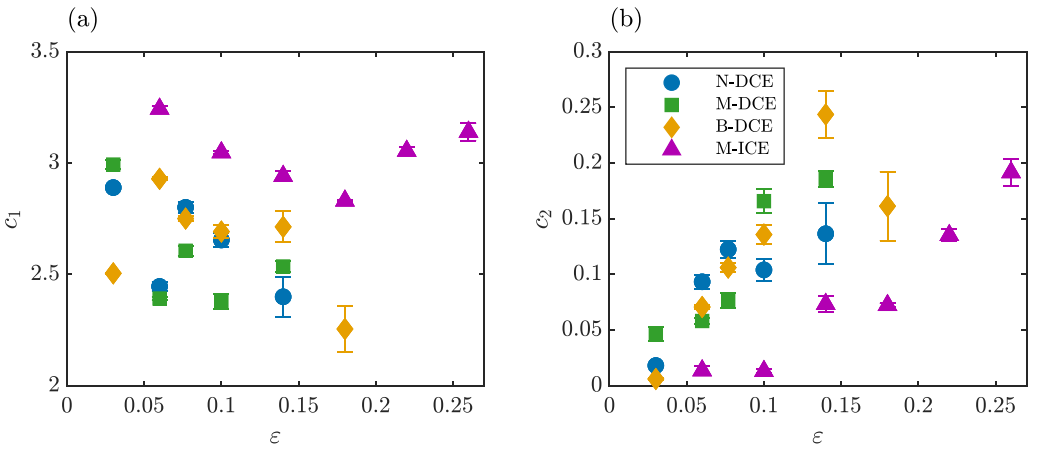

FIG. 16. Values of (a) c_1 and (b) c_2 from quadratic structure function scaling $\zeta(p) = c_1 p - (c_2/2)p^2$ vs ε for all experiments. Structure functions are calculated over the final 5 min of wavemaker forcing and averaged over all wave gauges. Error bars represent 95% confidence intervals on the quadratic fit.

within this range to determine the relationship between $\zeta(p)$ and p. To illustrate how $\zeta(p)$ changes with forcing intensity, we plot $\zeta(p)$ vs p for all M-DC experiments.

For small p (Fig. 15), we see $\zeta(p)$ similar to the simple scaling $\zeta(p) = p(|\nu| - 1)/2$. For higher values of p the behavior changes, strongly indicative of intermittency in the signal [39]. In particular, we observe that $\zeta(p)$ becomes more nonlinear as ε increases. Previous work has attempted to relate the asymptotic behavior of $\zeta(p)$ at large p to the underlying nonlinear structures. The classical model, used in [37], applies a linear fit $\zeta(p) = 2 - D + ap$, where a expresses the shape of singular crests and D gives their fractal dimension. This approach is not admissible to our results, which would return negative values of D. This issue may arise because of our choice of fourth-order increments [1].

Falcon *et al.* [39] and Deike *et al.* [12] used fourth-order increments, and instead of using a linear fit, they fit $\zeta(p)$ across all p by a quadratic fit $\zeta(p) = c_1 p - (c_2/2)p^2$, where c_2 is a measure of intermittency [40]. We apply the same approach here and find the quadratic fit to agree well with our results, shown in Fig. 16. For the weakest forcing from the N-DC and B-DC the lower bound of τ was raised to 0.1 to compensate for noise. To test the impact of intermittency, we calculate c_1 and c_2 for each experiment. Across all experiments, regardless of f_p and Δf, we observe a more nonlinear shape of $\zeta(p)$ as ε increases. Regarding the specific parameters of the power law, we find that c_1 generally decreases with increasing forcing, while c_2 increases. Falcon *et al.* [39] and Deike *et al.* [12] observed the same tendency, with values of c_1 and c_2 similar to our observations. As a nonzero value of c_2 is a sign of intermittency, its growth with ε suggests that the growth in forcing intensity yields a more nonlinear wave field. The role of intermittency in our resulting spectra can be gleaned from noting that $S_2(\tau)$ gives $|\nu| = 2(c_1 - c_2) + 1$. Therefore, we can deduce that the reduction in ν with increasing forcing is at least partially driven by stronger nonlinearities, since c_2 increases with ε.

IV. CONCLUSION

We set out to create an idealized wave environment that met the assumptions of WT theory. By creating a wave field that is isotropic, weakly nonlinear, and of random phases, we created an optimal system for the weakly nonlinear energy transfers. However, we found that real-world effects that arise in a (round) physical laboratory were still significant, and interfered with the desired physics. We measured considerable dissipation at low frequencies, which provided a sink located

between the injection frequency and the inertial range. Consequently, energy was lost from these modes before it could be moved downscale by resonances, which may be why we observed steeper high-frequency tail than WT theory predicts.

We found that the slopes of the high-frequency tails we measured were strongly related to the intensity of the forcing, which has been well documented experimentally [4,11–15]. At low forcing intensity, the comblike spectra reflect a wave field dominated by harmonics. The higher harmonics peaks then flatten into smoother tails when the forcing steepness is increased. In particular, we observed a more efficient development of a spectral power law for broader forcing bandwidths and higher values of ε. This agrees with the numerical work of Zhang and Pan [26]. In general, our spectra tended towards f^{-6} for the widest and strongest forcing, which corresponds to mesoscopic turbulence due to finite-size effects [8].

At frequencies less than our forcing, some of the spectra developed a power law over a thin frequency range, but at a flatter slope than the theoretical $f^{-11/3}$. While prior gravity wave experiments have observed nonresonant three-wave interactions [14,15,41], recent studies in circular domains reveal the potential for resonant triads in the presence of rotation [42] or at specific depths [43], which inhibit the formation of an inverse cascade. We cannot directly quantify the impact of three-wave interactions in our system, but they may affect both cascades.

After the wavemakers are turned off, the system enters a freely decaying regime. Our spectra do not decay self-similarly, but rather undergo exponential decay, consistent with energy loss primarily due to dissipation. While our results disagree with a power-law decay from WT theory, there are prior numerical [44] and experimental [45] results of WT in different systems which also decay exponentially under significant dissipation.

Our dissipation features more aggressive decay at low frequencies, particularly at 1.3 Hz. This frequency lies between the peak frequency and its second harmonic for the DC experiments. The quick decay at 1.3 Hz leads to the reappearance of the second harmonic at later times across all experiments, with higher harmonics reemerging for low ε. For the IC experiments, 1.3 Hz lies below the peak frequency, but it still decays more quickly than neighboring frequencies. In both cases, this represents a removal of energy from the system near the start of the inertial range: at the low-frequency end of the forward cascade and the high-frequency end of the inverse cascade. We suspect, but cannot prove, that waves at this frequency are absorbed by the wavemakers, given that the length scale of these waves is roughly equal to twice the width of a wave paddle.

We examined increments of our time series and observed that the relation between the spectral power laws and forcing intensity may be partially due to an increase in intermittent events. The evolution of our PDFs revealed that our wave field deviates significantly from a random system, particularly for larger ε. The behavior of our structure functions was captured well by a quadratic fit, with an intermittency coefficient c_2 that grew with ε. By relating the structure functions to the spectral power law, we suspect that stronger nonlinearities helped flatten the spectral slopes. Without spatial data, we cannot identify why we have intermittent events in our signal. The cause of intermittency in WT is an open question, but there are possible origins related to sharp-crested waves [37], whitecapping [46], gravity-capillary wave interactions [47], or breaking waves [48]. From our time series across all experiments, our extreme values of $\delta_\eta^4(\tau)$ seem to occur when a large amplitude wave group passes by a probe, resulting in extreme variations in η over a short time interval. Our intermittency did not seem to coincide with wave breaking or parasitic capillary waves, which is consistent with [39]. Nevertheless, our work emphasizes the need to incorporate intermittency into the WT model.

Finite-size effects, dissipation, and intermittency are each considerable obstacles towards producing an idealized wave turbulent system in a laboratory environment. Our findings present the sensitivity of the system to artificial factors, which must be considered when designing an experimental system.

ACKNOWLEDGMENTS

Z.T. and A.S. were supported by NSF, Grants No. OCE-2405801, No. OCE-2049213, and No. OCE-1736989. M.O. was funded by Progetti di Ricerca di Interesse Nazionale (PRIN) (2020X4T57A and 2022WKRYNL) and by the Simons Foundation (Award No. 652354).

[1] S. Nazarenko and S. Lukaschuk, Wave turbulence on water surface, Annu. Rev. Condens. Matter Phys. **7**, 61 (2016).
[2] L. D. Talley, *Descriptive Physical Oceanography: An Introduction* (Academic, New York, 2011).
[3] G. J. Komen, L. Cavaleri, M. Donelan, K. Hasselmann, S. Hasselmann, and P. Janssen, *Dynamics and Modelling of Ocean Waves* (Cambridge University Press, Cambridge, NY, 1996).
[4] E. Falcon and N. Mordant, Experiments in surface gravity–capillary wave turbulence, Annu. Rev. Fluid Mech. **54**, 1 (2022).
[5] S. Nazarenko, *Wave Turbulence*, Lecture Notes in Physics, Vol. 825 (Springer Science & Business Media, Berlin, Germany, 2011).
[6] G. Falkovich, *Fluid Mechanics: A Short Course for Physicists* (Cambridge University Press, Cambridge, UK, 2011).
[7] S. Badulin, A. Pushkarev, D. Resio, and V. Zakharov, Self-similarity of wind-driven seas, Nonlinear Processes Geophys. **12**, 891 (2005).
[8] V. S. L'vov and S. Nazarenko, Discrete and mesoscopic regimes of finite-size wave turbulence, Phys. Rev. E **82**, 056322 (2010).
[9] E. A. Kartashova, Weakly nonlinear theory of finite-size effects in resonators, Phys. Rev. Lett. **72**, 2013 (1994).
[10] M. Onorato and G. Dematteis, A straightforward derivation of the four-wave kinetic equation in action-angle variables, J. Phys. Commun. **4**, 095016 (2020).
[11] A. Campagne, R. Hassaini, I. Redor, J. Sommeria, T. Valran, S. Viboud, and N. Mordant, Impact of dissipation on the energy spectrum of experimental turbulence of gravity surface waves, Phys. Rev. Fluids **3**, 044801 (2018).
[12] L. Deike, B. Miquel, P. Gutiérrez, T. Jamin, B. Semin, M. Berhanu, E. Falcon, and F. Bonnefoy, Role of the basin boundary conditions in gravity wave turbulence, J. Fluid Mech. **781**, 196 (2015).
[13] S. Lukaschuk, S. Nazarenko, S. McLelland, and P. Denissenko, Gravity wave turbulence in wave tanks: Space and time statistics, Phys. Rev. Lett. **103**, 044501 (2009).
[14] P. Cobelli, A. Przadka, P. Petitjeans, G. Lagubeau, V. Pagneux, and A. Maurel, Different regimes for water wave turbulence, Phys. Rev. Lett. **107**, 214503 (2011).
[15] A. Campagne, R. Hassaini, I. Redor, J. Sommeria, and N. Mordant, The energy cascade of surface wave turbulence: Toward identifying the active wave coupling, in *Turbulent Cascades II: Proceedings of the Euromech-ERCOFTAC Colloquium 589* (Springer, New York, 2019), pp. 239–246.
[16] B. Issenmann and E. Falcon, Gravity wave turbulence revealed by horizontal vibrations of the container, Phys. Rev. E **87**, 011001(R) (2013).
[17] S. Galtier, *Physics of Wave Turbulence* (Cambridge University Press, Cambridge, UK, 2022).
[18] E. A. Kuznetsov, Turbulence spectra generated by singularities, JETP Lett. **80**, 83 (2004).
[19] A. O. Korotkevich, Simultaneous numerical simulation of direct and inverse cascades in wave turbulence, Phys. Rev. Lett. **101**, 074504 (2008).
[20] S. Y. Annenkov and V. I. Shrira, Direct numerical simulation of downshift and inverse cascade for water wave turbulence, Phys. Rev. Lett. **96**, 204501 (2006).
[21] A. O. Korotkevich, Inverse cascade spectrum of gravity waves in the presence of a condensate: A direct numerical simulation, Phys. Rev. Lett. **130**, 264002 (2023).
[22] E. Falcon, G. Michel, G. Prabhudesai, A. Cazaubiel, M. Berhanu, N. Mordant, S. Aumaître, and F. Bonnefoy, Saturation of the inverse cascade in surface gravity-wave turbulence, Phys. Rev. Lett. **125**, 134501 (2020).

[23] M. McAllister, T. Adcock, P. Taylor, and T. Van Den Bremer, The set-down and set-up of directionally spread and crossing surface gravity wave groups, J. Fluid Mech. **835**, 131 (2018).
[24] M. L. McAllister, S. Draycott, T. Adcock, P. Taylor, and T. Van Den Bremer, Laboratory recreation of the Draupner wave and the role of breaking in crossing seas, J. Fluid Mech. **860**, 767 (2019).
[25] S. Draycott, T. Davey, D. Ingram, A. Day, and L. Johanning, The SPAIR method: Isolating incident and reflected directional wave spectra in multidirectional wave basins, Coastal Eng. **114**, 265 (2016).
[26] Z. Zhang and Y. Pan, Numerical investigation of turbulence of surface gravity waves, J. Fluid Mech. **933**, A58 (2022).
[27] H. Socquet-Juglard, K. Dysthe, K. Trulsen, H. E. Krogstad, and J. Liu, Probability distributions of surface gravity waves during spectral changes, J. Fluid Mech. **542**, 195 (2005).
[28] S. Y. Annenkov and V. I. Shrira, "Fast" nonlinear evolution in wave turbulence, Phys. Rev. Lett. **102**, 024502 (2009).
[29] M. J. Tucker and E. G. Pitt, *Waves in Ocean Engineering* (Elsevier Science, Oxford, UK, 2001), Vol. 5.
[30] V. E. Zakharov, V. S. L'vov, and G. Falkovich, *Kolmogorov Spectra of Turbulence I: Wave Turbulence* (Springer Science & Business Media, Berlin, Germany, 2012).
[31] V. Zakharov, Statistical theory of gravity and capillary waves on the surface of a finite-depth fluid, Eur. J. Mech. B: Fluids **18**, 327 (1999).
[32] M. Onorato, A. R. Osborne, M. Serio, D. Resio, A. Pushkarev, V. E. Zakharov, and C. Brandini, Freely decaying weak turbulence for sea surface gravity waves, Phys. Rev. Lett. **89**, 144501 (2002).
[33] L. Deike, M. Berhanu, and E. Falcon, Decay of capillary wave turbulence, Phys. Rev. E **85**, 066311 (2012).
[34] V. E. Zakharov, Energy balance in a wind-driven sea, Phys. Scr. **T142**, 014052 (2010).
[35] E. Falcon, S. Fauve, and C. Laroche, Observation of intermittency in wave turbulence, Phys. Rev. Lett. **98**, 154501 (2007).
[36] E. Falcon, S. G. Roux, and B. Audit, Revealing intermittency in experimental data with steep power spectra, Europhys. Lett. **90**, 50007 (2010).
[37] S. Nazarenko, S. Lukaschuk, S. McLelland, and P. Denissenko, Statistics of surface gravity wave turbulence in the space and time domains, J. Fluid Mech. **642**, 395 (2010).
[38] E. Falcon, Laboratory experiments on wave turbulence, Discrete Contin. Dyn. Syst. - Ser. B **13**, 819 (2010).
[39] E. Falcon, S. G. Roux, and C. Laroche, On the origin of intermittency in wave turbulence, Europhys. Lett. **90**, 34005 (2010).
[40] S. B. Pope, *Turbulent Flows* (Cambridge University Press, Cambridge, UK, 2006).
[41] G. Michel, B. Semin, A. Cazaubiel, F. Haudin, T. Humbert, S. Lepot, F. Bonnefoy, M. Berhanu, and É. Falcon, Self-similar gravity wave spectra resulting from the modulation of bound waves, Phys. Rev. Fluids **3**, 054801 (2018).
[42] G. Michel, Three-wave interactions among surface gravity waves in a cylindrical container, Phys. Rev. Fluids **4**, 012801(R) (2019).
[43] M. Durey and P. A. Milewski, Resonant triad interactions of gravity waves in cylindrical basins, J. Fluid Mech. **966**, A25 (2023).
[44] Y. Pan and D. K. Yue, Decaying capillary wave turbulence under broad-scale dissipation, J. Fluid Mech. **780**, R1 (2015).
[45] L. Deike, J.-C. Bacri, and E. Falcon, Nonlinear waves on the surface of a fluid covered by an elastic sheet, J. Fluid Mech. **733**, 394 (2013).
[46] C. Connaughton, S. Nazarenko, and A. C. Newell, Dimensional analysis and weak turbulence, Physica D (Amsterdam, Neth.) **184**, 86 (2003).
[47] M. Berhanu, E. Falcon, and L. Deike, Turbulence of capillary waves forced by steep gravity waves, J. Fluid Mech. **850**, 803 (2018).
[48] N. Yokoyama, Statistics of gravity waves obtained by direct numerical simulation, J. Fluid Mech. **501**, 169 (2004).